Supplemental Figure 1

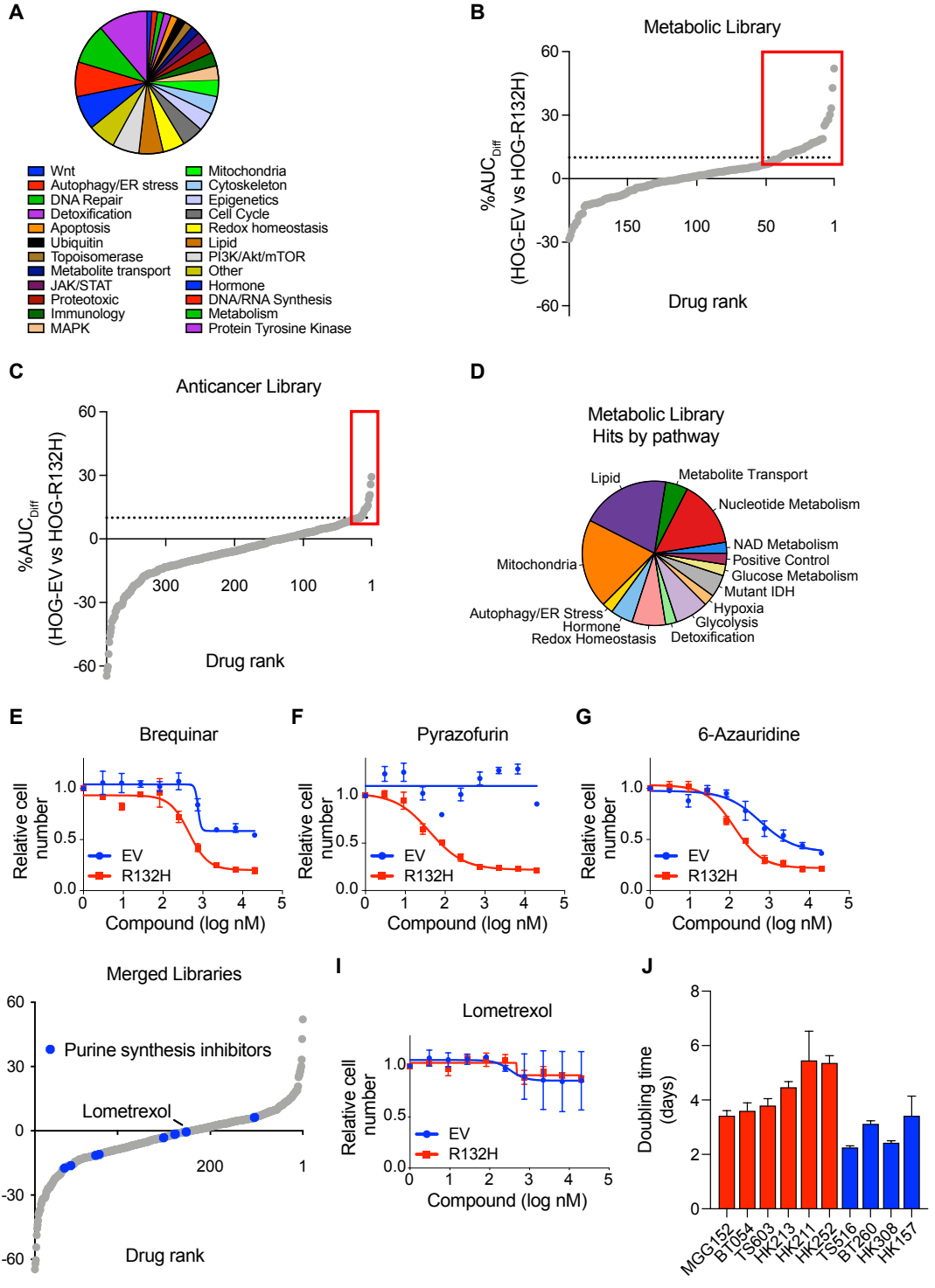

Supplemental Figure 2

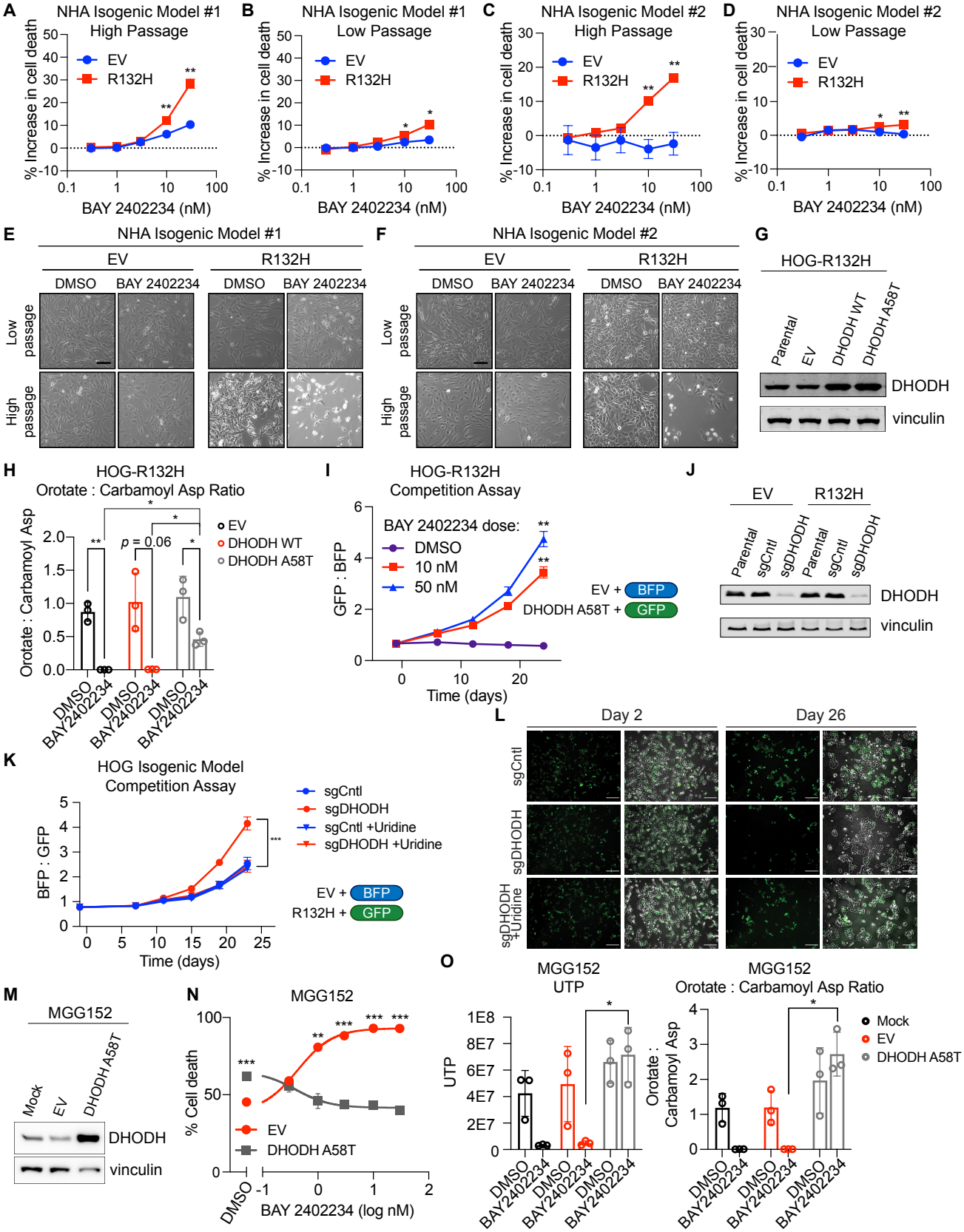

Supplemental Figure 3

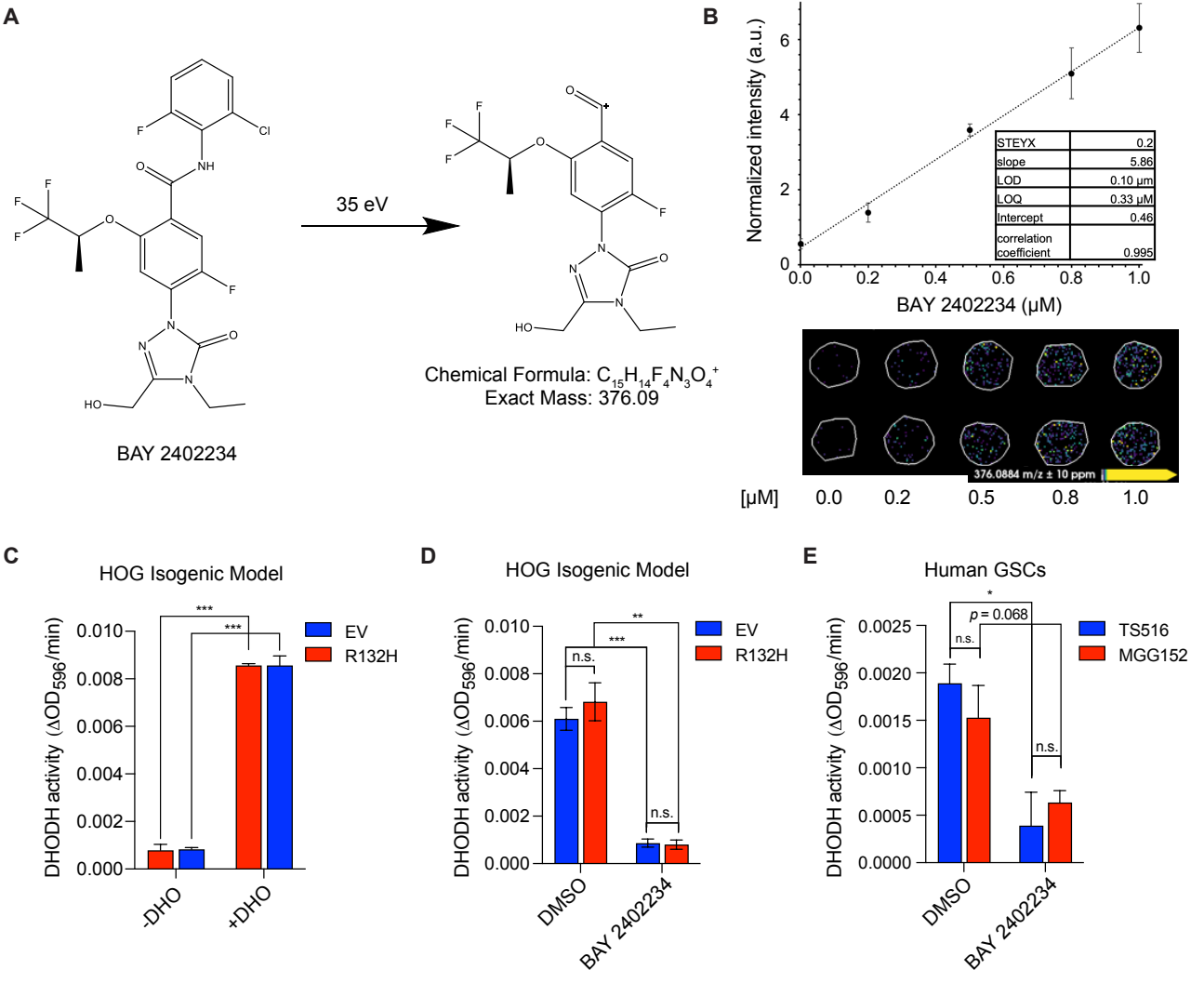

Supplemental Figure 4

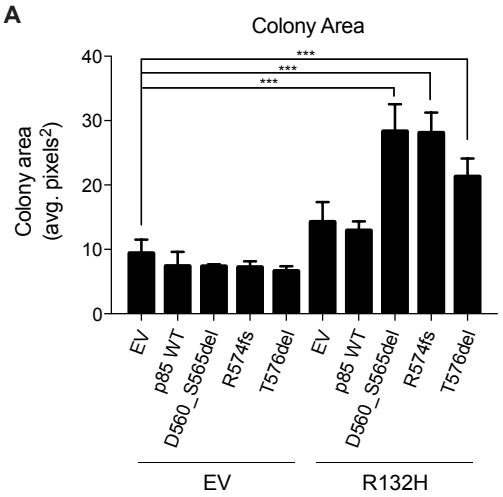

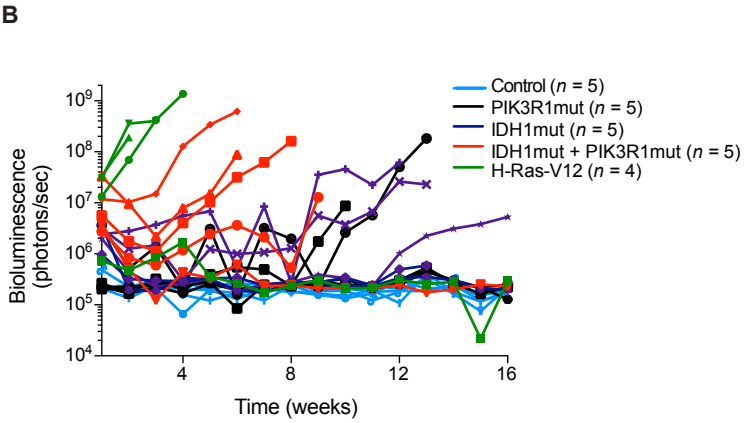

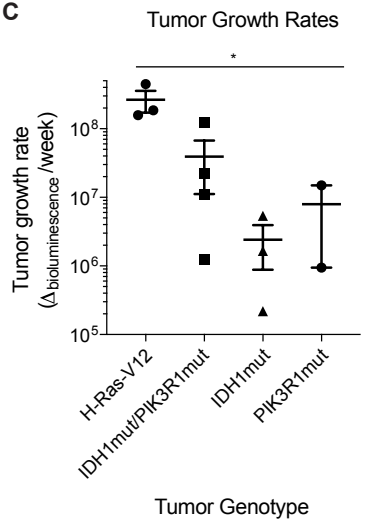

Supplemental Figure 5

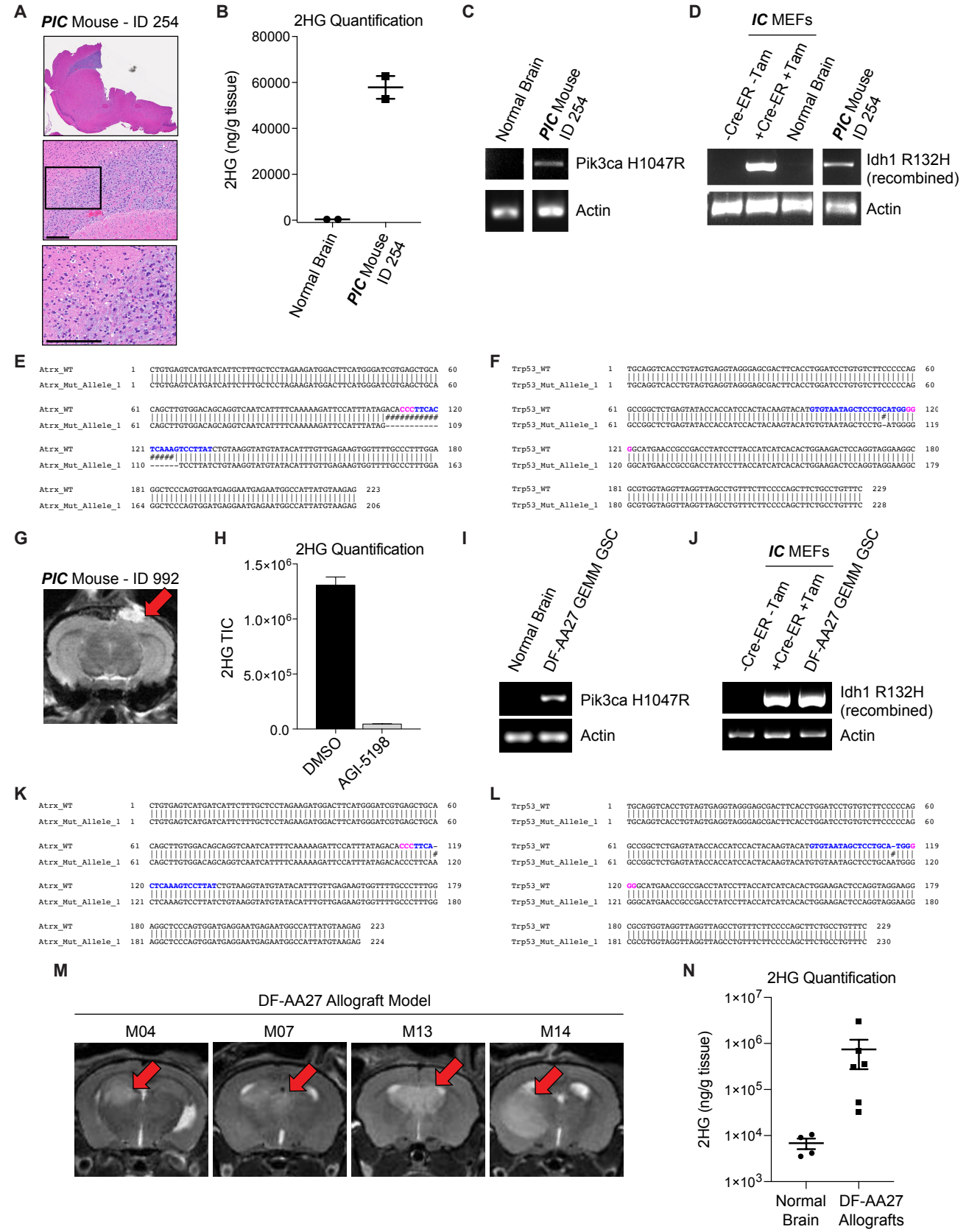

Supplemental Figure 6

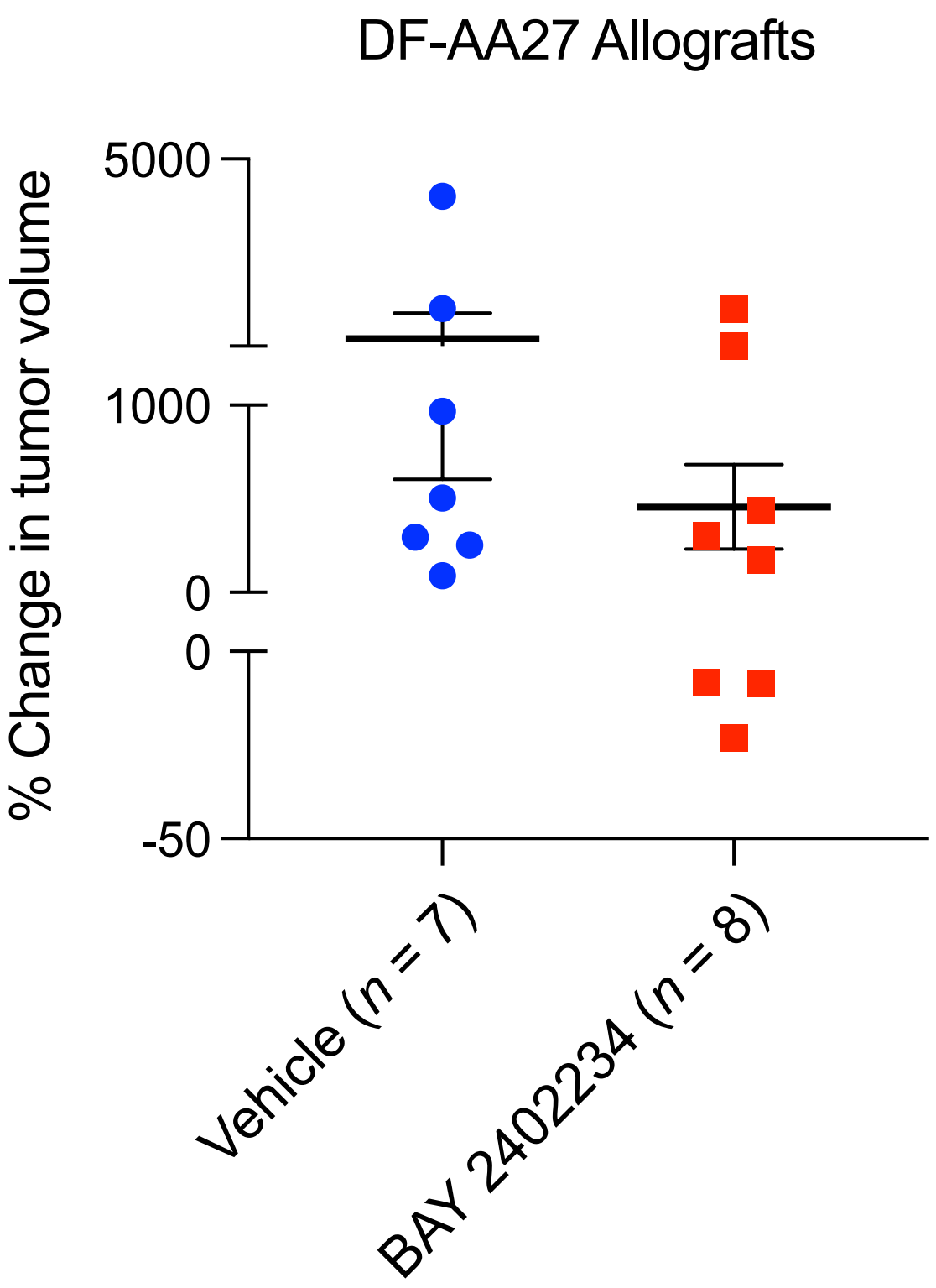

Supplemental Figure 7

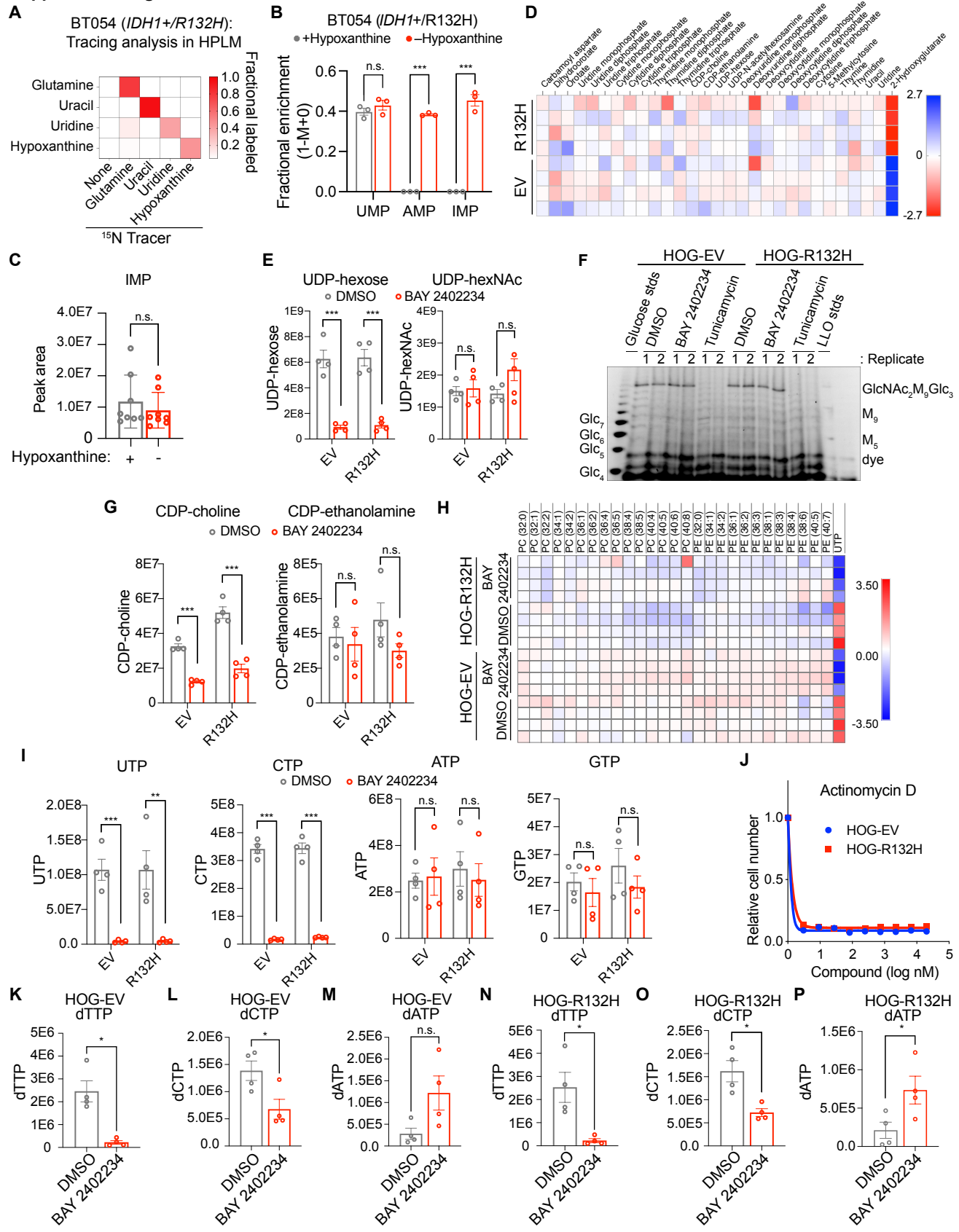

Supplemental Figure 8

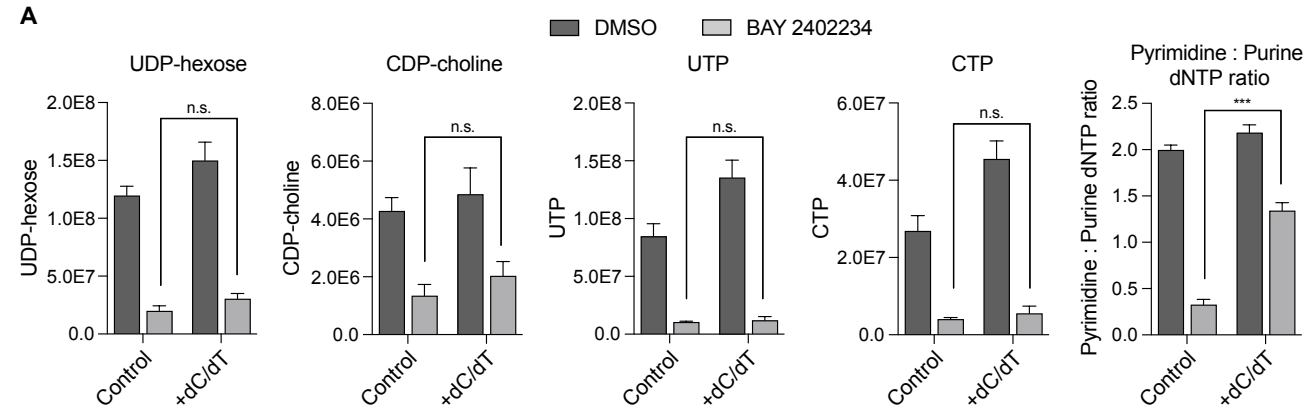

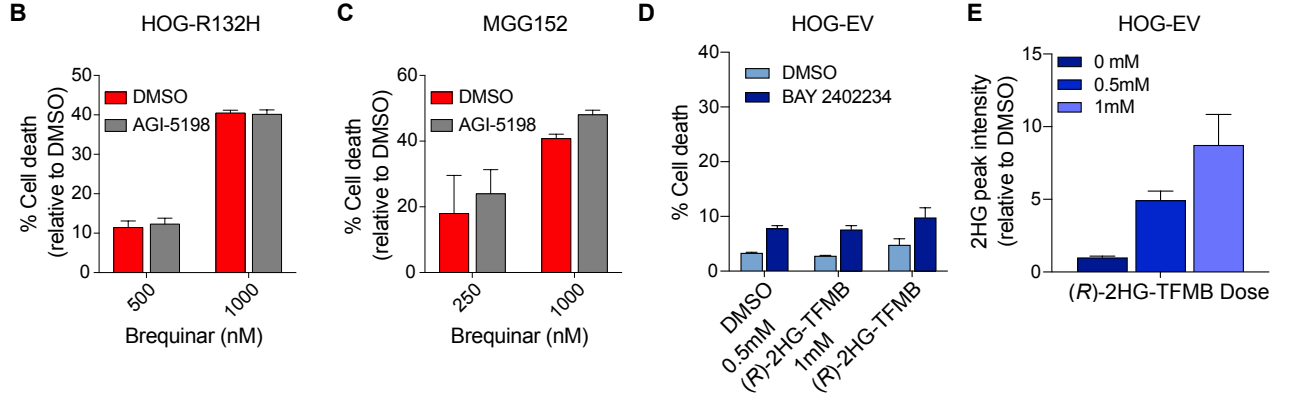

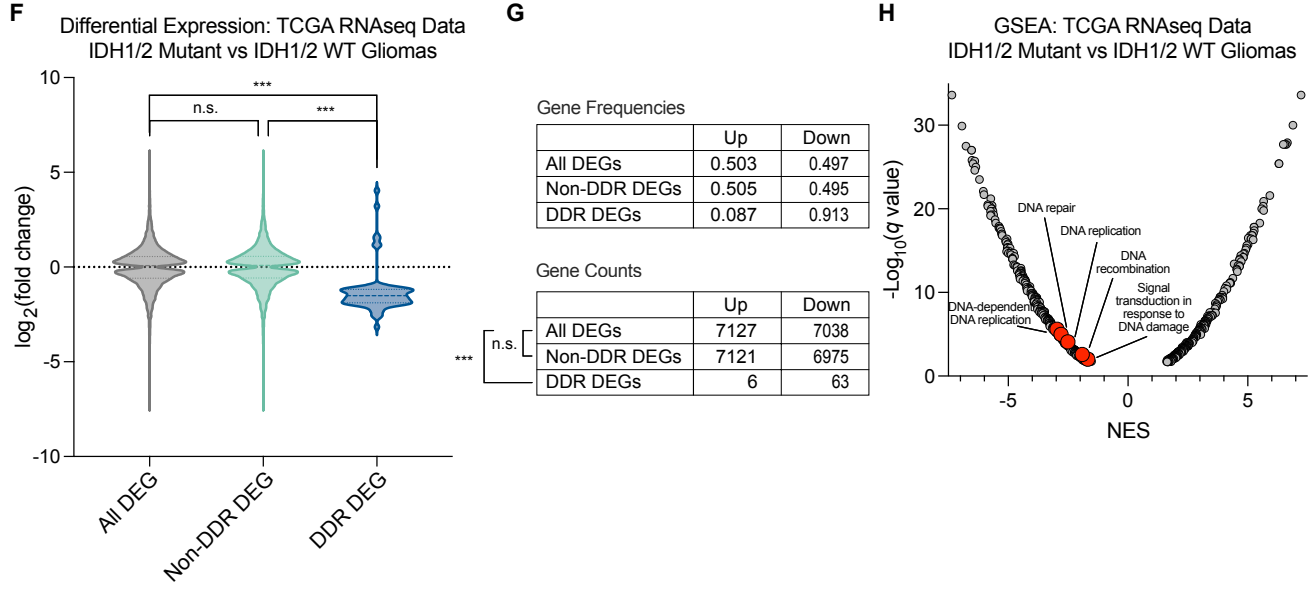

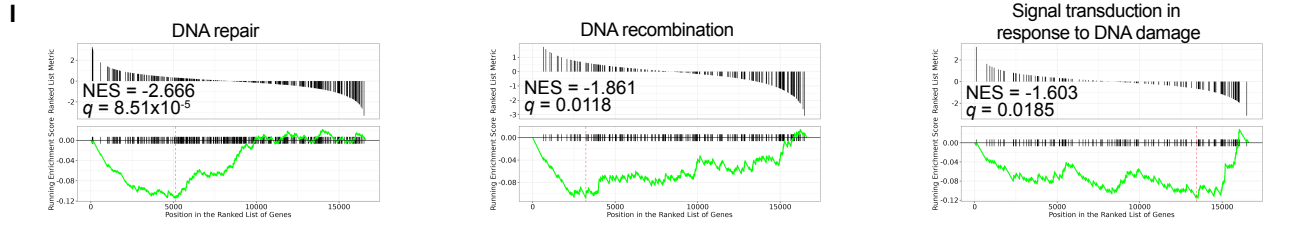

Table S2. Genotypes of glioma stem-like cell lines

Cell line	IDH1 status	TP53 status	Additional known alterations	Source
MGG152	IDH1-R132H	Mutant	MGMT methylated, *N-Myc* amplification	Wakimoto et al., 2014
BT054	IDH1-R132H	WT	1p19q co-deleted, 11q amplification	Kelly et al., 2014
TS603	IDH1-R132H	Unknown	1p19q codeleted	Rohle et al., 2013
HK213	IDH1-R132H	Mutant	*CDKN2A* copy number loss (-1), *ATRX* copy number loss (-2), 1p19q intact	Laks et al., 2016; Garrett et al., 2018
HK211	IDH1-R132H	Mutant	*EGFR* vIII, *CDKN2A* copy number loss (-2), 1p19q intact	Laks et al., 2016; Garrett et al., 2018
HK252	IDH1-R132H	Mutant	*PTEN* copy number loss (-1), *ATRX* copy number loss (-1), *CDKN2A* copy number loss (-1), 1p19q intact	Laks et al., 2016; Garrett et al., 2018
TS516	WT	Unknown	Unknown	Rohle et al., 2013
BT260	WT	Unknown	1p19q codeleted	Koivunen et al., 2012
HK308	WT	Mutant	*EGFR* vIII	Laks et al., 2016; Garrett et al., 2018
HK157	WT	WT	*EGFR* amplified, *ATRX* copy number loss (-1), *CDKN2A* copy number loss (-2)	Laks et al., 2016; Garrett et al., 2018

Table S3. Genetic Alterations Co-Occurring and Mutually Exclusive with IDH1 Mutations in Glioma

			Lower Grade Glioma (TCGA, Provisional)		Glioblastoma (TCGA, Provisional)	
Gene 1	Gene 2	Association	p-Value	Log Odds Ratio	p-Value	Log Odds Ratio
IDH1	TP53	Co-Occurrence	< 0.001	> 3.00	< 0.001	> 3.00
IDH1	ATRX	Co-Occurrence	< 0.001	> 3.00	< 0.001	> 3.00
IDH1	CIC	Co-Occurrence	< 0.001	2.155	0.048	> 3.00
IDH1	PIK3R1	Co-Occurrence*	0.134	1.991	0.011	2.431
IDH1	PIK3CA	None	0.411	-0.289	0.536	-0.700
IDH1	PTEN	Mutual Exclusivity	< 0.001	< -3.00	< 0.001	< -3.00

*Statistically significant co-occurrence observed only in glioblastoma study.

SUPPLEMENTAL INFORMATION

SUPPLEMENTAL FIGURE LEGENDS

Figure S1. Drug Screen in IDH1 Mutant and IDH1 WT Glioma Cells, Related to Figure 1. (A) Pie chart depicting pathways targeted by drugs in the metabolic and anticancer libraries. (B and C) Waterfall plot of drugs screened from the metabolic library (B) and the anticancer library (C). Hits were determined by plotting relative cell number by dose of each drug tested for both HOG-EV and HOG-R132H cells and calculating the areas under each curve (AUCs). $\%AUC_{Diff}$ values in HOG-EV and HOG-R132H cells were calculated for all drugs. Drugs with $>10\%AUC_{Diff}$ (dotted line) were categorized as hits (red outline). (D) Pie chart depicting pathways targeted by hits in the metabolic library used in (B). (E–G) Drug screen results for HOG-EV and HOG-R132H cells treated with brequinar (E), pyrazofurin (F), or 6-azauridine (G). (H) Waterfall plot of drugs from the metabolic and anticancer libraries with purine synthesis inhibitors highlighted in blue. (I) Drug screen results, as in (E–G), for lometrexol, an inhibitor of de novo purine synthesis. (J) Doubling times of IDH1 mutant (MGG152, BT054, TS603, HK213, shown in red) and IDH wild-type (TS516, BT260, HK308, HK157, shown in blue) GSC lines. For HK211, $n = 2$; for all others, $n = 3$. For all panels, data are means ± SEM.

Figure S2. Validation in Additional Isogenic Models and Genetic Validation of On-Target Efficacy of BAY 2402234, Related to Figure 2. (A–D) Cell death assays of two normal human astrocyte (NHA) isogenic models (NHA model #1, A–B and NHA model #2, C–D) expressing either empty vector (EV) or mutant IDH1 (R132H) treated with BAY 2402234 at the indicated doses for 4 days (NHA model #1) or 6 days (NHA model #2) ($n = 3$ in each panel). (E)

Representative photomicrographs of cells in (A) and (B). (F) Representative photomicrographs of cells in (C) and (D). For (E) and (F), scale bars = 100 μm. (G) Immunoblot analysis of HOG-R132H cells expressing an empty vector (EV), DHODH WT, or a drug-resistant DHODH (DHODH A58T). (H) Ratio of orotate to carbamoyl aspartate in the cells as in (G) treated with 50 nM BAY 2402234 or DMSO for 24 hours (n = 3). (I) Ratio of GFP to BFP in HOG-R132H cells expressing either BFP or DHODH A58T-IRES-GFP, mixed, and dosed with either the indicated concentrations of BAY 2402234 or DMSO. Cells were plated on Day -1 and dosed with BAY 2402234 or DMSO on Day 0 (n = 3). (J) Immunoblot analysis of HOG-EV or HOG-R132H cells with or without expression of Cas9 and an sgRNA targeting DHODH (sgDHODH) or a non-targeting control sgRNA (sgCntl). (K) Ratio of BFP to GFP in HOG cells expressing either EV and BFP or R132H and GFP, mixed, and infected with an sgRNA targeting DHODH or a non-targeting control sgRNA (sgCntl), with or without 100 μM uridine supplementation. Cells were plated on Day -1 and infected with lentivirus encoding Cas9 and one of the two sgRNAs on Day 0. Cells were maintained in either 100 μM uridine or DMSO. (L) Photomicrographs of the indicated cells and conditions described in (K). Scale bar = 100 μm. (M) Immunoblot analysis of MGG152 cells (Mock) or stable lines expressing EV or DHODH A58T. (N) Cell death assay in MGG152 cells as in (M) treated with the indicated concentrations of BAY 2402234 or DMSO (n = 3). (O) UTP and ratio of orotate to carbamoyl aspartate in MGG152 cell lines as in (M) treated with 30 nM BAY 2402234 or DMSO for 24 hours. Carbamoyl asp = carbamoyl aspartate. For panels (A–D, I, K, and N), data are means ± SEM. For panels (H and O), data are means ± SD. $p < .05$, $^{**}p < .01$, $^{***}p < .001$. Two-tailed p-values were determined by unpaired t-test.

Figure S3. In Vivo Assessment of On-Target Efficacy of BAY 2402234, Related to Figure 3. (A) Schema depicting ion transition used for MALDI MSI-based quantification of BAY 2402234. (B) Quantification (top) and images (bottom) of BAY 2402234 standard curve as assessed by MALDI-MSI in (A). STEYX: standard error; LOD = limit of detection; LOQ = limit of quantitation. (C) DHODH activity assay with or without addition of the DHODH substrate L-dihydroorotate (DHO) in HOG-EV and HOG-R132H cells. Activity was determined by isolating mitochondria and coupling DHODH activity to the redox dye 2,6-dichloroindophenol (absorbance: 596 nm) and measuring change in absorbance. (D) DHODH activity in HOG-EV (n = 3) and HOG-R132H (n = 3) cells treated with 10 nM BAY 2402234 or DMSO for 24 hours. DHODH activity was determined as in (C). (E) DHODH activity in MGG152 (IDH1 mutant) (n = 3) and TS516 (IDH1 WT) (n = 3) GSCs treated with 10 nM BAY 2402234 or DMSO for 24 hours. DHODH activity was determined as in (C) and (D). For all panels, data are means ± SEM; *p < .05, **p < .01, *** p < .001. In (C–E), two-tailed p-values were determined by unpaired t-test.

Figure S4. In Vitro and In Vivo Assessments of Transformation of Engineered Astrocytes, Related to Figure 4. (A) Average sizes of soft agar colonies formed by the indicated NHA cell derivatives 21 days after plating. NHA cells were infected to express HA-tagged IDH1-R132H [or with the empty vector (EV)] and then superinfected to express FLAG-tagged wild-type or mutant (D560_S565del, R574fs, or T576del) p85 (protein product of *PIK3R1* gene) or the corresponding EV. All cells were also infected to express firefly luciferase and GFP (n = 5 per group). (B) Quantification of brain bioluminescence after intracranial injection of astrocytes

expressing EV/EV (control), IDH1^{R132H}/EV (IDH1mut), EV/p85^{D560_S565del} (PIK3R1mut), IDH1^{R132H}/p85^{D560_S565del} (IDH1mut + PIK3R1mut), or H-Ras-V12 (as a positive control) as well as firefly luciferase and GFP. Bioluminescence imaging was performed once per week for 16 weeks; time 0 = one week post-tumor cell injection. (C) Quantification of xenograft tumor growth rates in mice described in (B). Mice that did not develop tumors or were not able to be imaged ≥ 2 times were censored because growth rates could not be calculated in these instances. For all panels, data are means ± SEM; *$p < .05$, *** $p < .001$. In (A), two-tailed p-values were determined by unpaired t-test. In (C), p-value was determined by one-way ANOVA.

Figure S5. Characterization of a GEM Model of Astrocytoma Driven by Mutant IDH1, Related to Figure 5. (A) Representative images from hematoxylin and eosin (H&E) stained sections of brain tissue from an AAV-injected ***PIC*** mouse. Higher magnification images show area of infiltrating tumor cells into normal brain parenchyma. Black box in middle panel indicates magnified region in lower panel; scale bars = 200 μm. (B) Absolute 2HG levels (measured by GC-MS) in tumor tissue extracted from the mouse brain shown in (A) and in normal mouse brain tissue (n = 2 per group). (C) RT-PCR assays for *PIK3CA^{H1047R}* transgene or *Actb* gene expression in tumor tissue extracted from the mouse brain shown in (A) and in normal mouse brain tissue. (D) Genomic DNA PCR assays to detect the recombined *LSL-Idh1-R132H* allele or *Actb* gene in tumor tissue extracted from the mouse brain shown in (A), normal mouse brain tissue, and in mouse embryonic fibroblasts (MEFs) lines derived from a naïve ***IC*** mouse. MEFs were transduced in vitro with retrovirus to express the tamoxifen-inducible MerCreMer recombinase and then treated with 4-hydroxytamoxifen or were mock transduced and untreated to serve as positive and negative controls, respectively. (E and F) CRISPR amplicon sequencing

of genomic DNA regions of *Atrx* (E) and *Trp53* (F) genes targeted by sgRNAs shown in Figure 5A in tumor tissue extracted from the mouse brain shown in (A). Dominant variant alleles identified in tumor tissue are aligned with wild-type gene sequences. PAM sites and sgRNA sequences are shown in pink and blue, respectively; # indicate mismatches and – indicate missing DNA bases. (G) Representative MRI image of an AAV-injected ***PIC*** mouse that developed a needle-track osteosarcoma at the injection site in the skull. (H) Relative 2HG levels (measured by GC-MS) in DF-AA27 GSCs treated with 3 μM AGI-5198 (a mutant IDH1 inhibitor) or DMSO for 72 hours; $n = 2$. TIC = total ion count. (I) RT-PCR assays for *PIK3CA*^{H1047R} transgene or *Actb* gene expression, as in (C), in DF-AA27 GSCs. (J) Genomic DNA PCR assays to detect the recombined *LSL-Idh1-R132H* allele or *Actb* gene, as in (D), in DF-AA27 GSCs. (K and L) CRISPR amplicon sequencing of genomic DNA regions of *Atrx* (K) and *Trp53* (L) genes in DF-AA27 GSCs, as in (E) and (F). (M) Representative MRI images of mouse brains with DF-AA27 allografts. Unique mouse IDs are shown above each image. (N) Absolute 2HG levels (measured by GC-MS) in DF-AA27 allografts ($n = 6$) and normal mouse brain ($n = 4$). For (G) and (M), MRI images are coronal slices of the entire mouse brain. For (B) and (H), data are means ± SD. For (N), data are means ± SEM.

Figure S6. In Vivo Validation of DHODH as a Therapeutic Target in an IDH-mutant GEMM-derived Allograft Mouse Model, Related to Figure 6. Percent changes in tumor volume as detected by MRI in DF-AA27 orthotopic allografts treated continuously with BAY 2402234 (4 mg/kg PO QD) or vehicle for 3 weeks following tumor formation. Data are means ± SEM.

Figure S7. Quantification of Protein Glycosylation, Phospholipid Synthesis, and RNA Synthesis Intermediates, Related to Figure 7. (A) ^{15}N stable isotope tracing assays using the indicated ^{15}N-labeled metabolites in human plasma-like medium (HPLM) (*n* = 3 per tracer). Heatmap depicts labeling of intracellular metabolite pools (y-axis) by tracers (x-axis) at 18 hours. (B) ^{15}N stable isotope tracing assay in BT054 (IDH1 mutant) cells. ^{15}N-labeled glutamine was administered to cells cultured in either standard human plasma-like medium (HPLM) or HPLM depleted of hypoxanthine for 5 days. Labeling of representative pyrimidine [uridine monophosphate (UMP)] and purine [adenosine monophosphate (AMP), inosine monophosphate, (IMP)] nucleotides was measured 18 hours later by LC-MS (*n* = 3 per group). (C) Steady state levels of IMP measured in BT054 (IDH1 mutant) cells cultured in either standard HPLM or HPLM depleted of hypoxanthine for 5 days. (D) Heatmap depicting relative levels of pyrimidine nucleotides in HOG-EV and HOG-R132H cells (*n* = 4 per group). 2-hydroxyglutarate is included as a positive control for a differentially regulated metabolite. (E, G, I) Relative quantification of protein glycosylation (E), phospholipid synthesis (G), and RNA synthesis (I) intermediates by LC-MS in HOG-EV and HOG-R132H cells treated with 10 nM BAY 2402234 or DMSO for 24 hours (*n* = 4). Values on y-axes are peak areas determined by LC-MS. (F) Fluorophore-Assisted Carbohydrate Electrophoresis (FACE) assay of lipid-linked oligosaccharides (LLOs) in HOG-EV and HOG-R132H cells treated with 10 nM BAY 2402234, 1 μg/mL tunicamycin, or DMSO for 24 hours (*n* = 2). Glucose oligomer and LLO standards (stds) are shown in the first lane and the second to last lane; Glc = glucose, M = mannose, GlcNAc = N-acetylglucosamine. Dolichol-linked $GlcNAc_2M_9Glc_3$ oligosaccharide (labeled at right) is a substrate for N-linked glycosylation and is not regulated by BAY 2402234 treatment. Tunicamycin, an inhibitor of N-linked glycosylation, depletes dolichol-linked $GlcNAc_2M_9Glc_3$

and serves as a positive control. (H) Heatmap depicting relative levels of phosphatidylcholine (PC) and phosphatidylethanolamine (PE) lipids in HOG-EV and HOG-R132H cells treated with 10 nM BAY 2402234 or DMSO for 24 hours (n = 4). UTP is a pharmacodynamic marker for DHODH inhibition and is included as a positive control. (J) MAPS drug screen results for HOG-EV and HOG-R132H cells treated with the mRNA synthesis inhibitor actinomycin D. Data are derived from drug screen depicted in Figure 1A–C. (K–P) Relative quantification of pyrimidine (dTTP, dCTP) and purine (dATP) deoxynucleotide triphosphate (dNTPs) levels by LC-MS in HOG-EV (K–M) and HOG-R132H (N–P) cells treated with 10 nM BAY 2402234 or DMSO for 24 hours (n = 4 per group). Values on y-axes are peak areas determined by LC-MS. For all panels, data are means ± SEM, *p < .05, **p < .01, ***p < .001, n.s. = not significant. Two-tailed p-values were determined by unpaired t-test.

Figure S8. Mechanistic Studies of De Novo Pyrimidine Synthesis Hyperdependence Induced by IDH Mutations, Related to Figure 8. (A) Relative quantification of protein glycosylation (UDP-hexose), phospholipid synthesis (CDP-choline), and RNA synthesis (UTP, CTP) intermediates and pyrimidine dNTPs by LC-MS in HOG-R132H cells treated with 10 nM BAY 2402234 or DMSO in the presence or absence of 15 μM deoxycytidine (dC) and 15 μM deoxythymidine (dT) for 24 hours (n = 4). (B and C) Cell death assays of HOG-R132H (B) and MGG152 (C) cells treated with the indicated doses of brequinar for 48 and 96 hours, respectively, with or without pre-treatment with the mutant IDH inhibitor AGI-5198. HOG-R132H cells were pre-treated with 3 μM AGI-5198 for 72 hours (n = 3); MGG152 cells were pre-treated with 110 nM AGI-5198 for 48 hours (n = 2). (D) Cell death assays of HOG-EV cells treated with 5 nM BAY 2402234 or DMSO for 48 hours. Cells were pre-treated with the

indicated doses of cell-permeable 2HG ester, (*R*)-2HG-TFMB, or DMSO for 3 hours and media were refreshed every 24 hours with freshly added drug, ester, and/or vehicle ($n = 2$). (E) Relative quantification of 2HG levels by GC-MS following treatment with the indicated doses of (*R*)-2HG-TFMB or DMSO for 5 hours as in (D) ($n = 2$). (F) Fold changes in expression of genes in TCGA RNA sequencing dataset that are differentially expressed (DEGs) in IDH1/2 mutant gliomas versus IDH1/2 WT gliomas. Genes related to the DNA damage response (DDR) were selected by representation in gene ontology sets related to the DNA damage response or checkpoint signaling. (G) Frequency of upregulation and downregulation among genes in TCGA RNA sequencing dataset that are differentially expressed in IDH1/2 mutant gliomas versus IDH1/2 WT gliomas. (H) Normalized enrichment scores (NES) for all gene ontology sets differentially expressed in TCGA RNA sequencing of IDH1/2 mutant gliomas versus IDH1/2 WT gliomas. Gene ontology sets related to DNA replication or repair are highlighted. (I) Gene set enrichment analysis of DNA repair, DNA recombination, and signal transduction in response to DNA damage pathways in IDH1/2 mutant gliomas versus IDH1/2 WT gliomas. NES = normalized enrichment score. For all panels, data are means ± SEM. ***$p < .001$, n.s. = not significant. Two-tailed *p*-values were determined by unpaired *t*-test (A–E). In (F and G), mean fold changes were compared between groups by one-way ANOVA followed by post-hoc Tukey's multiple comparisons *t*-test between all groups. In (H and I), differential expression analysis was performed using the R package limma (Ritchie et al., 2015).

SUPPLEMENTAL TABLE LEGENDS

Table S2. Genotypes of Glioma Stem-like Cell Lines, Related to Figure 1. Known genetic alterations of IDH1 mutant and IDH WT glioma stem-like cell lines (GSCs) used in Figure 1.

Table S3. Genetic Alterations Co-Occurring and Mutually Exclusive with IDH1 Mutations in Glioma, Related to Figure 4. Analysis of associations between genetic alterations in *IDH1* and *TP53, ATRX, CIC, PIK3R1, PIK3CA,* and *PTEN* from The Cancer Genome Atlas (TCGA) Lower Grade Glioma (n = 283) and Glioblastoma (n = 585) datasets. One-sided p-values were determined by one-sided Fisher exact test. *indicates statistically significant co-occurrence observed only in Glioblastoma study.